Int. J. Electrochem. Sci., 15 **(2020)** 3776 – 3792, doi: 10.20964/2020.05.38

International Journal of
ELECTROCHEMICAL
SCIENCE
www.electrochemsci.org

Non-centrosymmetric $Na_7Li_{0.8}K_{0.2}Co_5(As_3O_{10})_2(As_2O_7)_2$: synthesis, structure and alkali ion-conduction pathways simulation

Riadh Marzouki [1,2,3,*], *Mohamed Faouzi Zid*[2]

[1] Chemistry Department, College of Science, King Khalid University, Abha 61413, Saudi Arabia.
[2] Laboratory of Materials, Crystal Chemistry and Applied Thermodynamics, LR15ES01, Faculty of Sciences of Tunis, University of Tunis El Manar, 2092, Tunisia.
[3] Chemistry Department, Faculty of Sciences of Sfax, University of Sfax, 3038, Tunisia.
[*]E-mail: riadh.marzouki@hotmail.fr, rmarzouki@kku.edu.sa

Received: 5 November 2019 / *Accepted:* 15 February 2020 / *Published:* 10 April 2020

A novel di-triarsenate material $Na_7Li_{0.8}K_{0.2}Co_5(As_3O_{10})_2(As_2O_7)_2$ has been synthesized by solid state reaction route. The structural study determined by single crystal X-ray diffraction showed the non-centrosymmetry of the structure. It crystallizes in the monoclinic system of C2 space group with the unit cell parameters: a=10.136(2) Å, b=8.722(2) Å, c=16.952(3) Å, β=101.86 (2)°, V= 1466.9(5)Å^3 and Z=2. Structural analysis using Charge Distribution (CHARDI) and Bond-Valence Sum (BVS) calculations tools are envisaged to confirm the proposed structural model. The $[Co_2O_{10}As_3O_{10}]_\infty$ chains connected to triarsentae groups toughen by CoO_6 octahedra forms a 3D anionic framework showing different tunnels, where alkali ions are located. Bond Valence Site Energy (BVSE) computational model was used to simulate the alkali-ion migration pathways in the anionic framework of the studied material. It shows that the alkali ion-conduction is probably ensured by sodium cations with an activation energy Ea= 0.83 eV. Only Na^+ ions migration is probably along [100] direction which diffuse through an infinite 1D pathway.

Keywords: Di-triarsenate, crystal structure, non-centrosymmetric, anionic framework, alkali-ion migration.

1. INTRODUCTION

The exploration of new materials in the *A*-*M*-*X*-O systems (*A*=Alkali; *M*= transition metals; *X*=P; Si; As) with three-dimensional anionic frameworks, showing large tunnels used for electrochemical applications, is an area of powerful activity in solid state chemistry [1-8]. The attention of several teams focused on phosphate compounds with remarkable thermal stability [9]. On

the other hand, a great structural similarity between phosphates and arsenates materials are shown due the possibility of partial or total substitution of phosphor by Arsenic [10].

Alkali cobalt arsenate are few compared to phosphates. In fact, the most studied family was β-Xenophillite with general formula $A_4Co_7(AsO_4)_6$ (*A* = Na; Ag) [11, 12] that behave fast ionic conductors. The second family has an olivine structure with general formula $ACoAsO_4$ (*A* = Li, Na, K) [13, 14]. Electrochemical performances were evaluated for these materials. It was the first electrochemical study on arsenates with olivine structure. Structural transition from olivine to spinel structure was observed by applying high pressure (8 GPa) at 1073 K [13]. This phase transition is also carried out under the same conditions with other transition metals (Fe, Ni and Mn) having the same degree of oxidation (+II).

The structural diversity, the interesting electrical and electrochemical properties of arsenates and their similarity to phosphates have prompted us to explore the *A*-Co-As-O systems that are sparsely studied.

In this paper, we investigate the synthesis, structural study and alkaline migration pathways of the new di-triarsenate $Na_7Li_{0.8}K_{0.2}Co_5(As_3O_{10})_2(As_2O_7)_2$.

2. EXPERIMENTAL AND COMPUTATIONAL METHODS

2.1. Synthesis

The novel alkali-cobalt arsenate material was synthesized by solid-state reaction method. A mixture of $NaNO_3$ (Sigma-Aldrich, ≥99.5%); (Sigma-Aldrich, ≥99.0%), $(Co(CH_3COO)_2.4H_2O$ (Merck, 99.999%); As_2O_5 (Merck, 99%) finely ground in an agate mortar in molar ratio 8: 5 : 10 is placed in a porcelain crucible. Firstly, it was heated at 673 K overnight to evaporate nitrate, acetate and water. In the next step, the residue was grounded and heated at 943 K for one week. After slowly cooling with 5K/min rate, pink crystals were obtained and isolated using boiling distilled water. After observing the obtained crystals under a polarizing microscope, a single crystal was selected for single crystal X-ray diffraction.

2.2. Single crystal X-ray diffraction

A suitable single crystal, with 0.2×0.16×0.15 mm^3 dimensions, was selected for X-ray diffraction data. The structural data were collected, at room temperature, on an Enraf-Nonius CAD-4 [15-16] diffractometer using the MoKα (λ=0.71073Å) radiation. The ordinary corrections; for Lorentz and polarization effects, absorption via a psi-scan [17] and secondary extinction correction [18] were applied. All subsequent calculations were carried out using the SHELX-97 [18] computer programs included in the WinGX software package [19]. Structure graphics were figured with Diamond 2 program [20].

2.3. Crystal structure validation tools

In order to confirm chemical composition and structural adopted model of the crystal structure resulting from the X-ray diffraction data analysis, two well-known models of structural validation were used, i.e. the Bond Valence Sum (BVS) [21] and Charge Distribution (CHARDI) [11]. The BVS and CHARDI calculations have been performed with the SoftBV [21] and CHARDI2015 [22] programs, respectively.

2.4. Pathways transport modeling

The cations motion in the anionic framework was studied via Bond Valence Site Energy (BVSE) model developed by Adams [23]. This model is the progress of BVS method model proposed by Pauling (1929) [24] to define the formation of inorganic compounds and later reformulated by Brown & Altermatt (1985) [25] with the following expression for an individual bond-valence $s_{A\text{-}X}$:

$$s_{A-X} = \exp\left(\frac{R_0 - R_{A-X}}{b}\right) \quad (1)$$

Where $R_{A\text{-}X}$ = distance between counter-ions A and X; R_0 and b= fitted constants, R_0 = length of a bond of unit valence

Recently, Mazza implemented the BVS model in the program Jumpiter to simulate the transport pathways of Na^+ in the NaSICON compound [26]. The most energetically favorable pathways of Na^+ are the points in the crystal structure where BVS is close to the formal oxidation number (i.e +1 for Na). Adams has developed this model further, relating the "valence units" to an energy scale by expressing the bond valence using a Morse-type interaction energy [23]. In brief, the pathway approach identifies regions of low site energy *E*(A):

$$E(\mathrm{A}) = D_0\left[\sum_{i=1}^{N}\left(\frac{s_{\mathrm{A-X_i}} - s_{\mathrm{min,A-X}i}}{s_{\mathrm{min,,A-X_i}}}\right)^2 - N\right] + E_{\mathrm{Coulomb}}\ (\mathrm{A-B}) \qquad (2)$$

Where the $E_{Coulomb}$ term describes the electrostatic interactions of the *A* cation with the anionic framework. For more details about the model and the mathematic equation, see the references [23].

The BVSE was used with success to simulate the transport pathways of Na^+ in $Na_4Co_7(AsO_4)_6$ [11] and $Na_{1.25}Co_{2.187}Al_{1.125}(AsO_4)_3$ [27] and Ag^+ in $Ag_{3.68}Co_2(P_2O_7)_2$ [28].

3. RESULTS AND DISCUSSION

3.1. Crystal structure determination and validation

After processing the raw data, the statistical calculation reveals that the structure is non-centrosymmetric and leads to the C2 space group. The direct method, included in the SHELXS-97 program, made it possible to locate cobalt, arsenic and some sodium and oxygen atoms. The rest of the atom positions contained in the unit cell were determined by successive Fourier-Difference syntheses

followed by a few cycles of refinements, based on the interatomic distances. The final refinement of all the anisotropic geometric and thermal parameters converges to the reliability factors of R=0.039 and wR=0.098. Moreover, the examination of the Fourier-Final Difference does not reveal any significant peak. The refinement results of the crystal structure are shown in Table 1.

Table 1. Crystal data refinement results of $Na_7Li_{0.8}K_{0.2}Co_5(As_3O_{10})_2(As_2O_7)_2$

Crystal data	
Empirical formula	$Na_7Li_{0.8}K_{0.2}Co_5(As_3O_{10})_2(As_2O_7)_2$
Crystal system ; Space group	Monoclinic; C2
Unit cell dimensions	a=10.136(2) Å, b=8.722(2) Å, c=16.952(3) Å, β=101.86 (2)°
Volume ; *Z*	1466.9(5) $Å^3$; 2
Formula weight ; $\rho_{calc.}$	1768.92 $gmol^{-1}$; 4.007 gcm^{-3}
Absorption coefficient (μ)	14.288 mm^{-1}
Crystal sharp ; color	Parallelepiped ; pink
Crystal size	0.2 × 0.16 × 0.15 mm
Data collection	
Diffractometer	Enraf-Nonius CAD-4
Wavelength ; Temperature	$\lambda_{Mo\ K\alpha}$=0.71069 Å ; 298(2) K
Theta range for data collection	2.46° ≤θ ≤ 26.97°
Limiting indices	-12 ≤*h*≤ 3 ; -11≤*k*≤ 1 ; -21 ≤*l*≤ 21
Scan mode	ω/2θ
Absorption correction ; T_{min} ; T_{max}	psi-scan ; 0.0806; 0.8614
Standards; frequency (min); decay (%)	2 ; 120 ; 1
Reflections collected	2452
Independent reflections	1913 [R_{int}= 0.050]
Observed reflections [$I > 2\sigma(I)$]	1738
Refinement	
Refinement method	Full-matrix least-squares on F^2
Final R indices [$I > 2\sigma(I)$]	R(F)= 0.039; wR(F^2)= 0.098,
Reflections ; parameters	1913 ; 290
$\Delta\rho_{max}$; $\Delta\rho_{min}$ ($eÅ^{-3}$)	0.98 ; -0.96
Goodness of fit (S)	1.06

The structural model of the adopted $Na_7Li_{0.8}K_{0.2}Co_5(As_3O_{10})_2(As_2O_7)_2$ formula is validated by CHARDI and BVS calculations. In fact, the resulted dispersion factors are σ_{cation} = 0.04 and σ_{anion} = 0.08; Then, the formal oxidation values are in good agreement with calculated charges Q(i) (Table 2).

Table 2. CHARDI and BVS analysis of ions in $Na_7Li_{0.8}K_{0.2}Co_5(As_3O_{10})_2(As_2O_7)_2$

Cation	V(i)	q(i).sof(i)	Q(i)	Anion	V(i)	q(i).sof(i)	Q
Co1	2.132	2.110	2.094	**O1**	-2.101	-2.000	-2.008
Co2	2.123	2.000	2.050	**O2**	-1.918	-2.000	-1.965
Co3	2.121	2.000	1.978	**O3**	-1.892	-2.000	-2.071
As1	4.990	5.000	5.106	**O4**	-2.019	-2.000	-1.948
As2	4.841	5.000	4.963	**O5**	-1.990	-2.000	-1.900
As3	4.826	5.000	5.095	**O6**	-1.964	-2.000	-1.890
As4	4.825	5.000	4.956	**O7**	-2.070	-2.000	-2.014
As5	4.879	5.000	4.924	**O8**	-2.225	-2.000	-2.080
Na1	0.991	1.000	1.025	**O9**	-2.142	-2.000	-2.075
Na2A	0.382	0.390	0.387	**O10**	-2.094	-2.000	-2.067
Na2B	0.607	0.610	0.619	**O11**	-2.210	-2.000	-1.868
Na3	1.005	1.000	0.987	**O12**	-1.983	-2.000	-1.879
Na4	0.204	0.200	0.199	**O13**	-2.097	-2.000	-1.954
Li4	0.799	0.800	0.794	**O14**	-2.108	-2.000	-1.960
Na5	0.641	0.630	0.632	**O15**	-2.342	-2.000	-2.115
K1	0.108	0.100	0.098	**O16**	-1.879	-2.000	-2.050
Na6	0.271	0.270	0.290	**O17**	-2.027	-2.000	-1.994

q(i)=Formal oxidation number; sof(i)=site occupation factor; Q(i)= computed charges

The fractional atomic coordinates and isotropic or equivalent isotropic displacement parameters are collected in Table 3.

Table 3. Fractional atomic coordinates and isotropic or equivalent isotropic displacement parameters (A^2)

Atom	x	y	z	U_{eq}*	Occ. (<1)
Co1	0.8442 (2)	0.4703 (2)	0.32950 (9)	0.0094 (4)	
Co2	0.3273 (2)	0.3476 (2)	0.31534 (9)	0.0095 (4)	
Co3	0	0.6672 (3)	0	0.0132 (5)	
As1	0.0535 (1)	0.1506 (2)	0.34617 (6)	0.0079 (3)	
As2	0.2784 (1)	0.4950 (2)	0.49187 (6)	0.0074 (3)	
As3	0.1378 (1)	0.6558 (2)	0.33147 (6)	0.0078 (3)	
As4	0.6992 (1)	0.4888 (2)	−0.00351 (7)	0.0100 (3)	
As5	0.8494 (1)	0.6395 (2)	0.15532 (6)	0.0101 (3)	
Na1	½	0.1919 (9)	½	0.014 (2)	
Na2A	0.732 (3)	0.675 (4)	0.8266 (13)	0.044 (4)	0.39 (2)
Na2B	0.759 (2)	0.579 (2)	0.8344 (8)	0.044 (4)	0.61 (2)
Na3	0.4376 (7)	0.4234 (8)	0.8286 (3)	0.0329 (9)	
Na4	0	0.311 (3)	½	0.021 (6)	0.20 (3)
Li4	0	0.311 (3)	½	0.021 (6)	0.80 (3)

Na5	−0.037 (2)	0.337 (2)	0.867 (2)	0.045 (4)	0.63 (3)
K1	0.519 (8)	0.829 (7)	0.135 (6)	0.045 (4)	0.10 (2)
Na6	−0.007 (3)	0.298 (3)	0.942 (2)	0.045 (4)	0.27 (1)
O1	0.8547 (9)	0.480 (1)	−0.0196 (5)	0.0170 (2)	
O2	0.8193 (9)	0.8070 (1)	0.1963 (5)	0.0150 (2)	
O3	0.4208 (7)	0.553 (1)	0.560 (5)	0.0143 (2)	
O4	−0.0074 (9)	0.654 (1)	0.1212 (5)	0.019 (2)	
O5	0.651 (1)	0.328 (1)	0.0359 (5)	0.018 (2)	
O6	0.1516 (7)	0.473 (1)	0.5392 (4)	0.008 (2)	
O7	0.8445 (9)	0.478 (1)	0.2084 (5)	0.015 (2)	
O8	−0.0600 (8)	0.045 (1)	0.2866 (5)	0.013 (2)	
O9	0.7073 (8)	0.624 (1)	0.0754 (4)	0.014 (2)	
O10	0.1633 (8)	½	0.2812 (5)	0.012 (2)	
O11	0.3238 (8)	0.354 (1)	0.4392 (5)	0.012 (2)	
O12	0.0020 (9)	0.317 (1)	0.3752 (5)	0.018 (2)	
O13	0.5917 (8)	0.566 (1)	−0.0805 (5)	0.016 (2)	
O14	0.1997 (8)	0.151 (1)	0.3151 (5)	0.011 (2)	
O15	−0.0182 (8)	0.6679 (12)	0.3513 (4)	0.0096 (8)	
O16	0.1852 (8)	0.816 (1)	0.2924 (5)	0.010 (2)	
O17	0.2446 (7)	0.655 (1)	0.4300 (4)	0.009 (1)	
$^{(*)}$Uéq = (1/3)$\sum_i\sum_j U^{ij} a_i^* a_j^* a_i.a_j$					

3.2. Crystal structure description

The asymmetric unit of $Na_7Li_{0.8}K_{0.2}Co_5(As_3O_{10})_2(As_2O_7)_2$ is presented in Figure 1. It contains three CoO_6 octahedra, As_2O_7 and As_3O_{10} groups connected by corners. The neutrality is assured by potassium and lithium ions located in the same site with sodium cations.

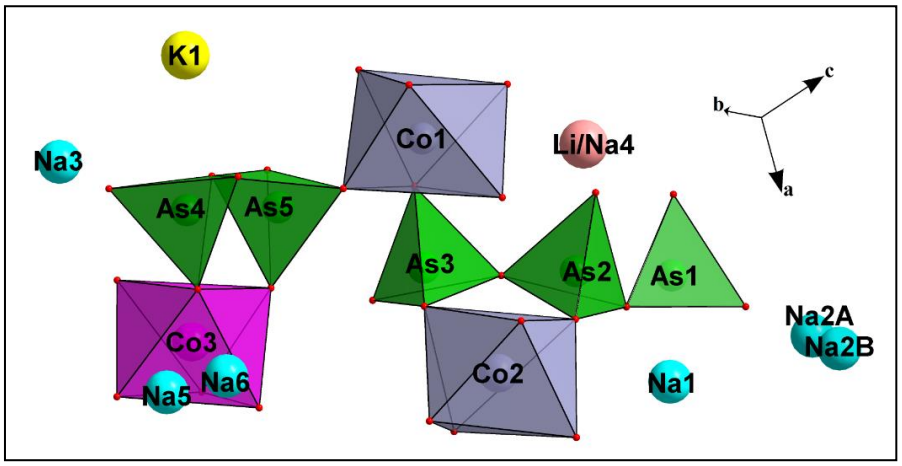

Figure 1. Asymmetric unit of $Na_7Li_{0.8}K_{0.2}Co_5(As_3O_{10})_2(As_2O_7)_2$, showing the atom labeling and the full coordination polyhedra including the corresponding symmetry-related O atoms**.**

In the anionic framework, The $Co1O_6$ and $Co2O_6$ octahedra share edges to form Co_2O_{10} dimers (Fig. 2a) which are connected together by triarsenate groups to form $[Co_2O_{10}As_2O_3]_\infty$ infinite chains in the *ab* plan (Fig. 2b).

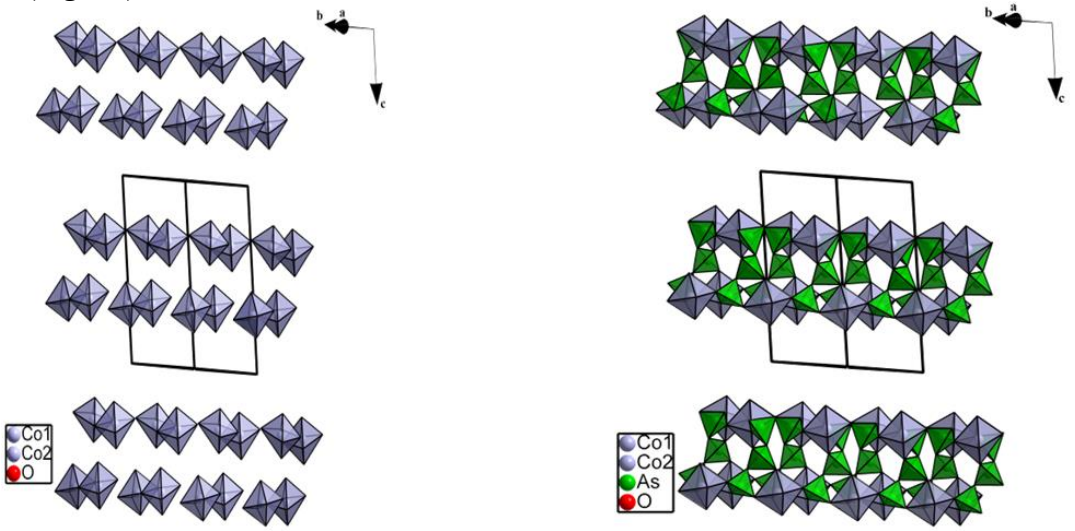

(a) (b)

Figure 2. Projection of (a) Co_2O_{10} dimers (b) $[Co_2O_{10}As_2O_3]_\infty$ infinite chains of $Na_7Li_{0.8}K_{0.2}Co_5(As_3O_{10})_2(As_2O_7)_2$.

The cohesion between chains is ensured by corners connection with the diarsenate groups As_2O_7 and, on the other side, by sharing corners with the $Co1O_6$ octahedra (Fig. 3).

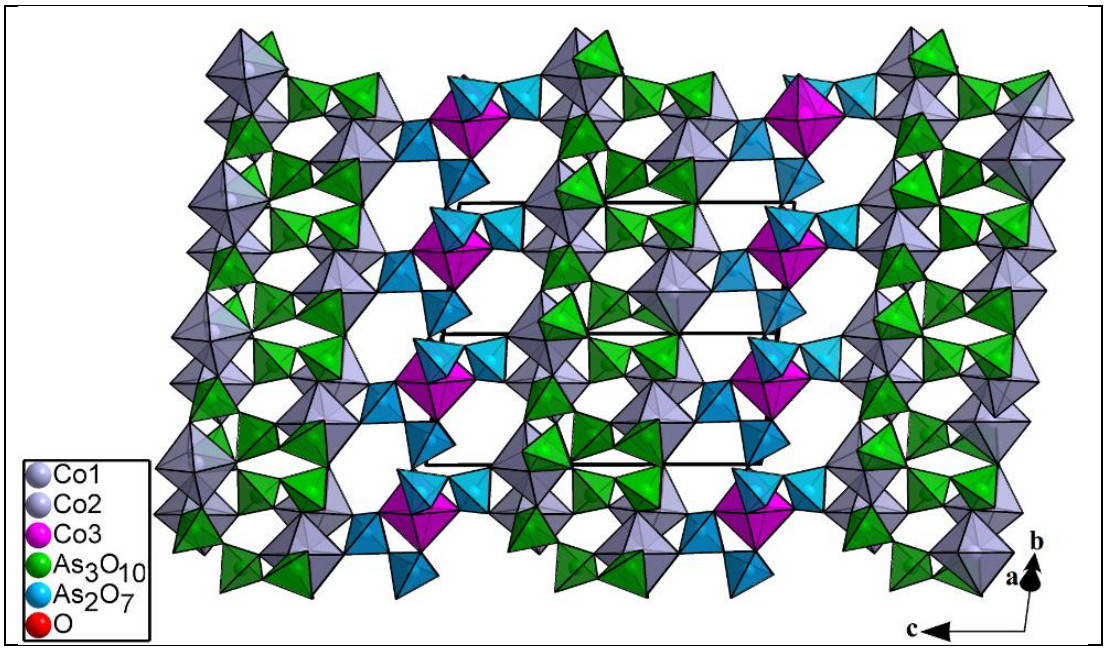

Figure 3. Projection close to the [100] direction showing the junction between layers of the *bc* plan in the anionic framework of $Na_7Li_{0.8}K_{0.2}Co_5(As_3O_{10})_2(As_2O_7)_2$.

It results a three-dimensional framework showing different types of tunnels along [100] (Fig. 4) and [010] (Fig. 5) where the alkali cations are located.

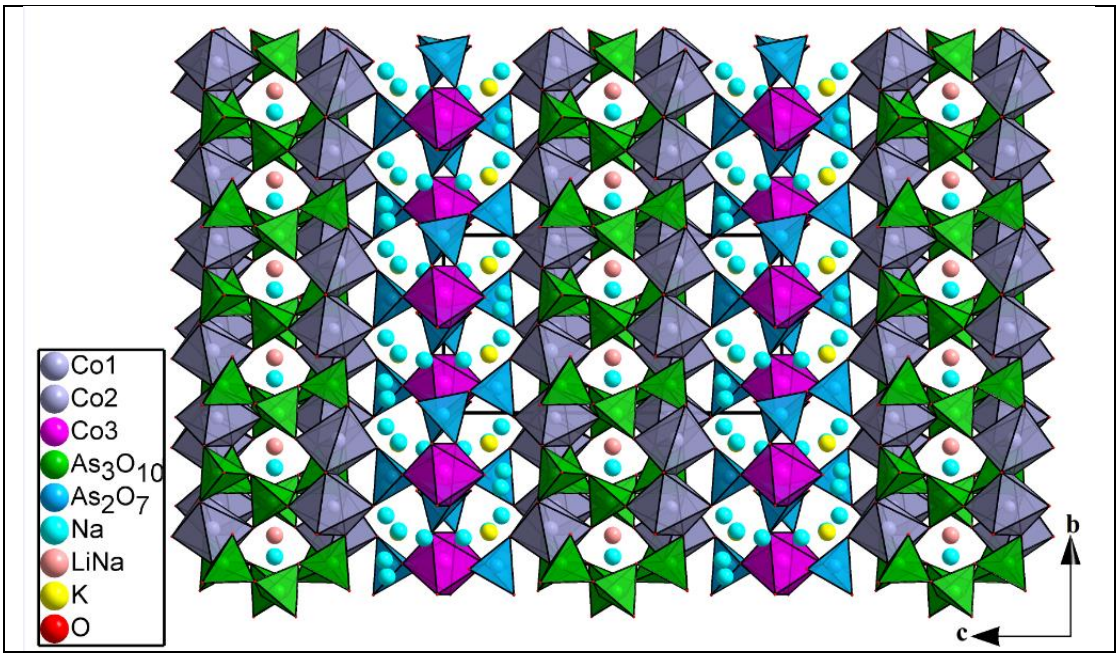

Figure 4. Projection of the $Na_7Li_{0.8}K_{0.2}Co_5(As_3O_{10})_2(As_2O_7)_2$ structure along [100] direction.

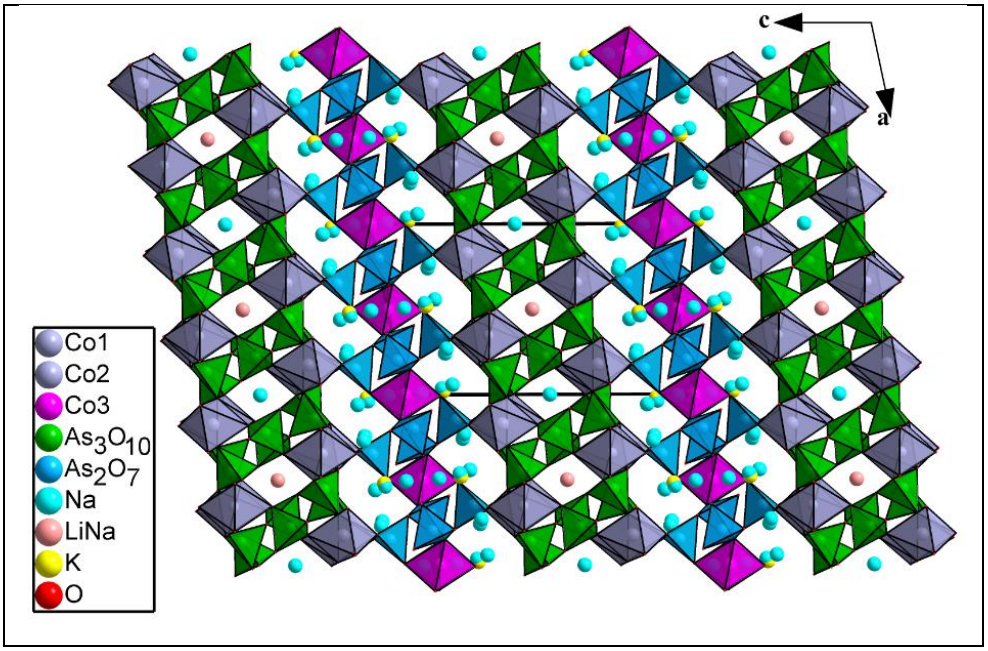

Figure 5. Projection of the $Na_7Li_{0.8}K_{0.2}Co_5(As_3O_{10})_2(As_2O_7)_2$ structure along [010] direction.

3.3. Crystallographic characteristics and comparison with other di-triarsenates materials:

By examining the structure of the title phase, the cobalt atoms are arranged in three crystallographic sites noted Co1, Co2 and Co3. Those possess an oxygenated octahedral coordination. However, the distortions values [29- 30] of the Co1-O, Co2-O and Co3-O bonds are 8.72%, 8.81% and 1.86%, respectively. It is well noted that the $Co1O_6$ and $Co2O_6$ octahedra are relatively much distorted. In fact, these octahedra are present as Co_2O_{10} dimers which cobalt atoms are displaced from the center of their octahedra in order to minimize the repulsive interactions between the common edge of the two octahedra. The Co-Co distance is equal to 3.286 (2) Å, hence the relatively high values of the link distortions. The Co-O interatomic distances in these octahedra are given in Table 4.

Table 4. Interatomic distances (Å) in CoO_6 octahedra.

$Co1O_6$		**$Co2O_6$**	
Co1—O7	2.054 (8)	Co2—O2^{v}	2.035 (9)
Co1—O16^{i}	2.093 (9)	Co2—O11	2.108 (8)
Co1—O12	2.110 (6)	Co2—O10	2.116 (9)
Co1—O14	2.130 (7)	Co2—O14	2.150 (6)
Co1—O15	2.200 (5)	Co2—O8^{vi}	2.178 (9)
Co1—O6^{iii}	2.218 (7)	Co2—O15	2.211 (9)
<Co1—O>	**2.134 (7)**	**<Co2—O>**	**2.133 (8)**

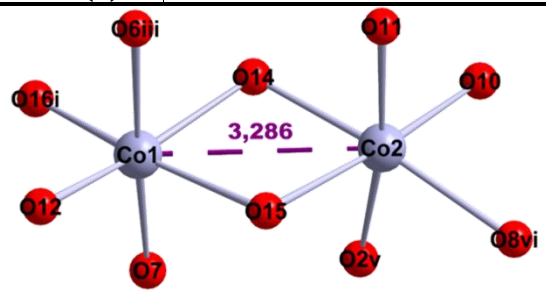

$Co3O_6$

Co3—O5^{vi}	2.075 (9)
Co3—O5^{viii}	2.075 (9)
Co3—O4^{ix}	2.075 (8)
Co3—O4	2.075 (8)
Co3—O1	2.179 (8)
Co3—O1^{ix}	2.179 (7)
<Co3—O>	**2.110 (8)**

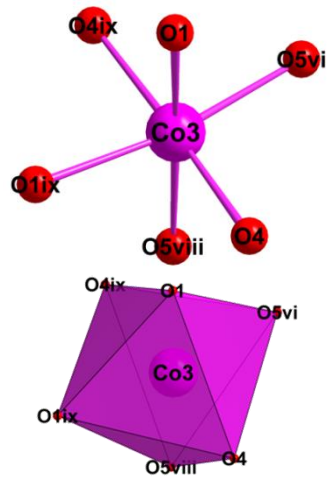

Symmetry codes (i) x−1/2, y−1/2, z; (iii) −x, y, −z+1; (v) −x−1/2, y−1/2, −z; (vi) x+1/2, y−1/2, z; (viii) −x, y, −z; (ix) −x−1/2, y+1/2, −z;

The As_2O_7 group, present in the asymmetric unit, is in pseudo-eclipsed conformation as shown in Figure 6. In fact, its pseudo-torsion angle is equal to 9.54 (4) ° for O1-As4-- As5-O4.

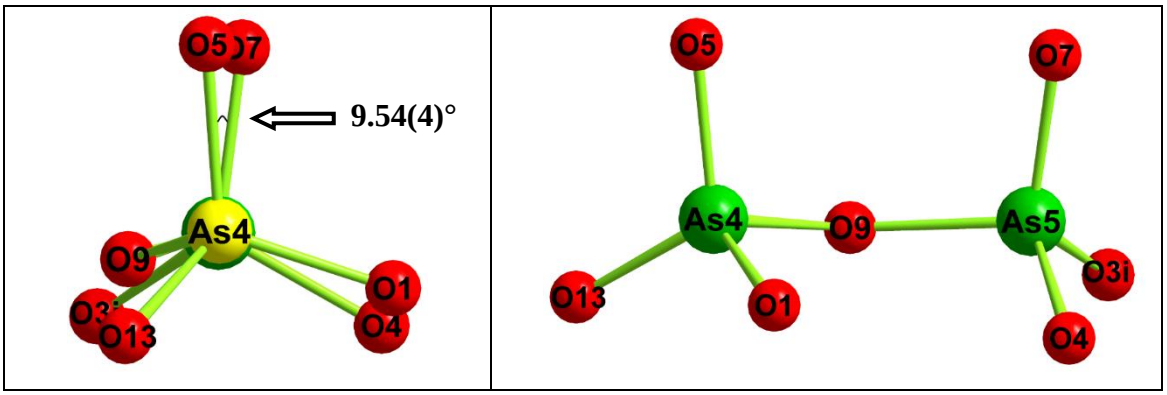

Figure 6. Conformation of diarsenate unit As_2O_7

While for the triarsenate unit, the two terminal AsO_4 tetrahedra located on either side at the ends of the As_3O_{10} group are in offset conformation, as shown in Figure 7a. Indeed, its torsion angle is equal to 27.81 (4) ° for O11-As2-As1-O8 and the central angle of the triarsenate As3 --- As2 --- As1 is 128.43 (3) ° (Fig. 7b).

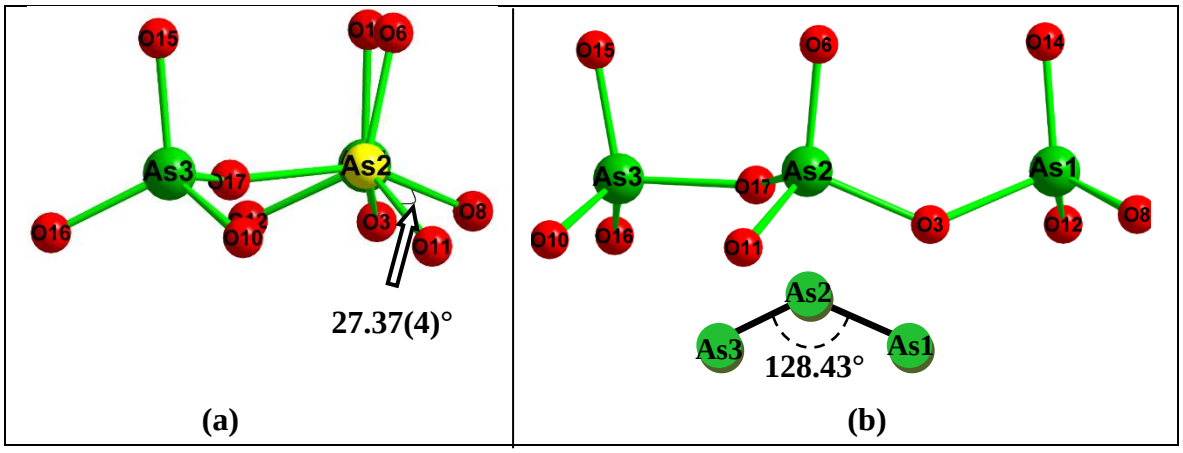

Figure 7. Conformation of triarsenate unit As_3O_{10}

By examining the bonds of the AsO_4 tetrahedra (Table 5), it is noted that the longest interatomic distances As-O are those of the oxygen atoms relative to the bridges of the As_2O_7 and As_3O_{10} groups. Their values are comparable to those found in the di-triarsenates $AMn_6(As_2O_7)_2(As_3O_{10})$ (A=K/Rb) [31-32].

Table 5. Interatomic distances (Å) in AsO4 tetrahedra

$Na_7Li_{0.8}K_{0.2}Co_5(As_3O_{10})_2(As_2O_7)_2$					
$As1O_4$		**$As2O_4$**		**$As3O_4$**	
As1—O12	1.659 (9)	As2—O11	1.640 (7)	As3—O10	1.645 (9)
As1—O8	1.659 (7)	As2—O6	1.662 (7)	As3—O16	1.671 (8)
As1—O14	1.675 (6)	As2—O3	1.722 (6)	As3—O15	1.692 (6)
As1—$O3^{vi}$	1.782 (7)	As2—O17	1.740 (7)	As3—O17	1.791 (6)
<As1—O>	**1.690 (7)**	**<As2—O>**	**1.691 (7)**	**<As3—O>**	**1.700 (7)**
$As4O_4$		**$As5O_4$**			
As4—O5	1.663 (9)	As5—O2	1.664 (9)		
As4—O13	1.665 (7)	As5—O7	1.685 (9)		
As4—O1	1.672 (7)	As5—O4	1.684 (7)		
As4—O9	1.777 (7)	As5—O9	1.762 (6)		
<As4—O>	**1.694 (8)**	**<As5—O>**	**1.699 (8)**		
$RbMn_6(As_2O_7)_2(As_3O_{10})$ [29]					
$As1O_4$		**$As2O_4$**			
As1—O4	1.670 (4)	As2-O4	1.670 (4)		
As1—O7	1.675 (4)	As2-O7	1.675 (4)		
As1—O3	1.676 (4)	As2-O3	1.676 (4)		
As1—O5	1.727 (4)	As2- O5	1.727 (4)		
<As1—O>	**1.687 (4)**	**<As2—O>**	**1.687 (4)**		
$As3O_4$		**$As4O_4$**			
As3—O12	1.655 (3)	As4—O2	1.651 (4)		
As3—O8	1.670 (4)	As4—$O9^{v}$	1.683 (3)		
As3—O10	1.676 (4)	As4—$O13^{v}$	1.684 (4)		
As3—O1	1.796 (4)	As4—O5	1.725 (4)		
<As3—O>	**1.699 (4)**	**<As4—O>**	**1.686 (4)**		

The difference between the studied structure and the di-triarsenates $AMn_6(As_2O_7)_2(As_3O_{10})$ structures (*A* = Rb or K) [29, 30] can be distinguished. In fact, in the structure of the studied material, the triarsenate groups provide the connection between the Co_2O_{10} dimers to form infinite layers parallel to the *ab* plane. The cohesion of these layers is ensured by sharing corners with the As_2O_7 diarsenates, on one side, and $Co1O_6$ octahedra, on the other side (Fig. 6a). However, in the $AMn_6(As_2O_7)_2(As_3O_{10})$ structure, the cohesion of the layers Mn_6O_{23}, arranged in "zigzag" in the [011] and [0-11] directions, is assured on the one hand, by sharing corners with As_2O_7 diarsenates and on the other hand, is reinforced by sharing corners with the As_3O_{10} triarsenates groups (Fig. 6b).

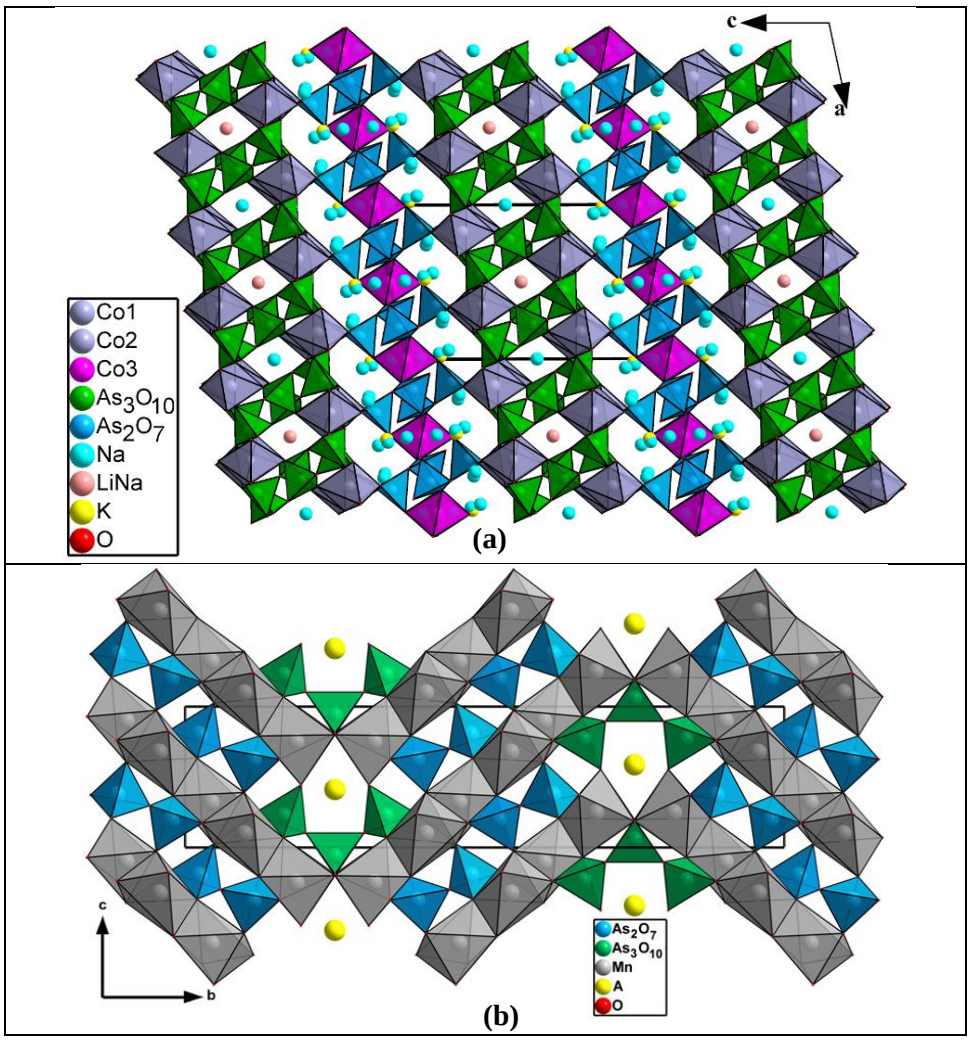

Figure 6. Projections of different types of bonds of As_2O_7 and As_3O_{10} groups in the structure of (a) $Na_7Li_{0.8}K_{0.2}Co_5(As_3O_{10})_2(As_2O_7)_2$ and (b) $AMn_6(As_2O_7)_2(As_3O_{10})$ where (A=Rb/K) [31-32]

According to the structural study, the title material has an open framework showing different tunnels, in both *a* and *b* directions, contain different disordered cations with relatively thermally agitations. These factors promote ionic conductivity which prompted us to study the alkali-ions pathways simulation in $Na_7Li_{0.8}K_{0.2}Co_5(As_3O_{10})_2(As_2O_7)_2$.

3.3. Alkali-ions Transport pathways simulation

The transport pathways modeling of Li; Na; and K cations in the anionic framework was carried out using the BVSE simulation model [23], based on the crystallographic data of the studied material.

Examination of isosurfaces connecting the sodium atom sites in the unit cell shows that only the sodium Na2A and Na2B can move along the [110] direction and form 1D infinite pathways (Fig. 7), although the calculated activation energy of about 0.83 eV suggests medium ionic conductivity. However, the other sodium atoms are blocked and cannot participate in the ionic conduction.

The conduction pathways simulated by the BVSE model are in good agreement with the structural characteristics of the studied material. Indeed, mobile sodium ions Na2A and Na2B are those located in the [110] direction. This direction corresponds to the direction of the tunnels having the widest sections ranging from 3.50(3) Å to 7.17(5) Å. On the other hand, the other alkali-ions are located in widows with lower sections. Figure 8 shows the different type of tunnels existing in the anionic framework of the title compound.

The conductivity of $Na_7Li_{0.8}K_{0.2}Co_5(As_3O_{10})_2(As_2O_7)_2$ (Ea=0.83 eV) is intermediate compared to other sodium-arsenate materials such as $Na_3Bi(AsO_4)_2$ (0.76 eV) [33] and $Na_3Bi_2(AsO_4)_3$ (0.85 eV) [34]. Nevertheless, the title compound is higher conductor than other sodium-based materials like as $Na_{5.2}Cu_{1.9}Al(AsO_4)_4$ (1.14 eV) [35]; $Na_2Co_2(MoO_4)_3$ (1.2 eV) [36]; $Na_{1.14}K_{0.86}CoP_2O_7$ (Ea= 1.34 eV) [37] and $Na_{2.84}Ag_{1.16}Co_2(P_2O_7)_2$ (Ea= 1.37 eV) [38]. On the other hand, $Na_7Li_{0.8}K_{0.2}Co_5(As_3O_{10})_2(As_2O_7)_2$ shows lower conductivity than other sodium ionic conductor like as Na-cellulose ($Ea_{393\text{-}458K}$ = 0.49 eV and $Ea_{458\text{-}500K}$= 0.68 eV) [39]; $Na_2CoP_{1.5}As_{0.5}O_7$ (0.563 eV) [40] $Na_4Co_{5.63}Al_{0.91}(AsO_4)_6$ (0.56 eV) [41] and $NaCo_2As_3O_{10}$ (Ea= 0.48 eV) [42].

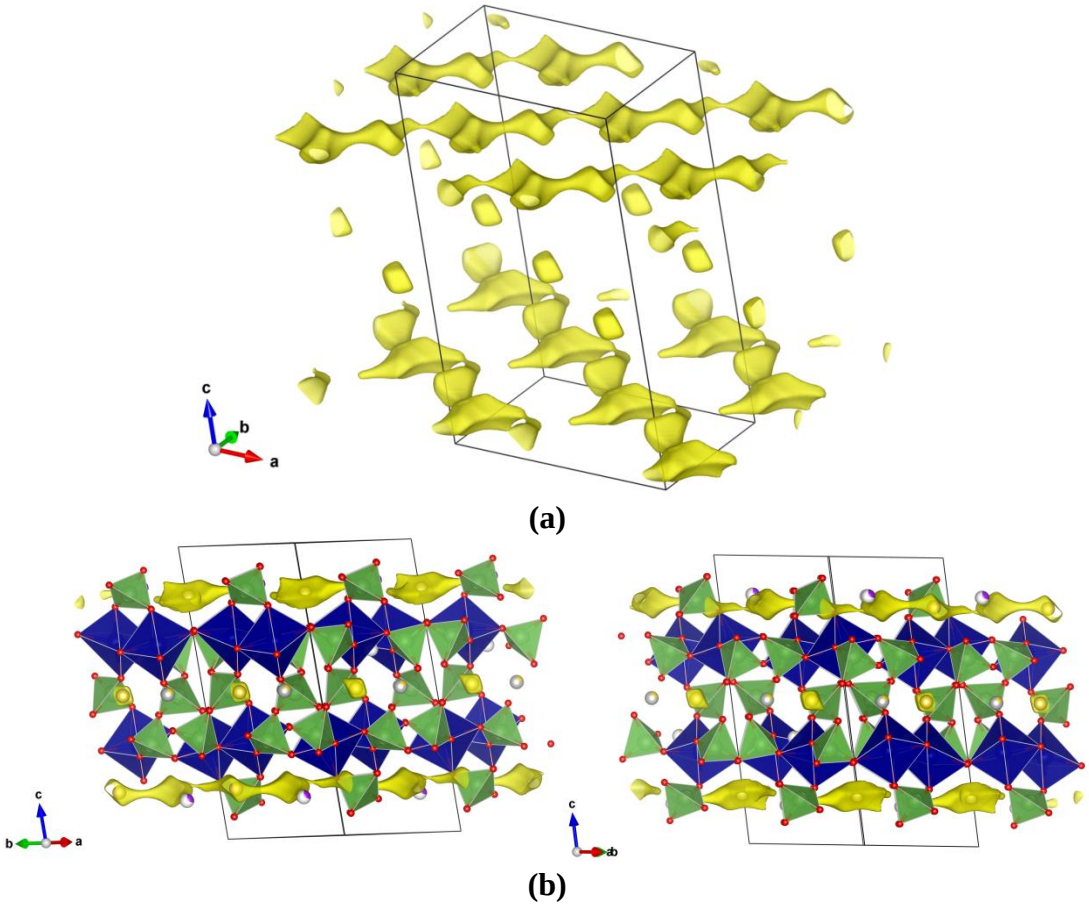

Figure 7. Projections of the unit cell of $Na_7Li_{0.8}K_{0.2}Co_5(As_3O_{10})_2(As_2O_7)_2$ showing the 1D infinite pathways of migration of sodium ions along [110] direction (a) without coordination polyhera and (b) with coordination polyhedra.

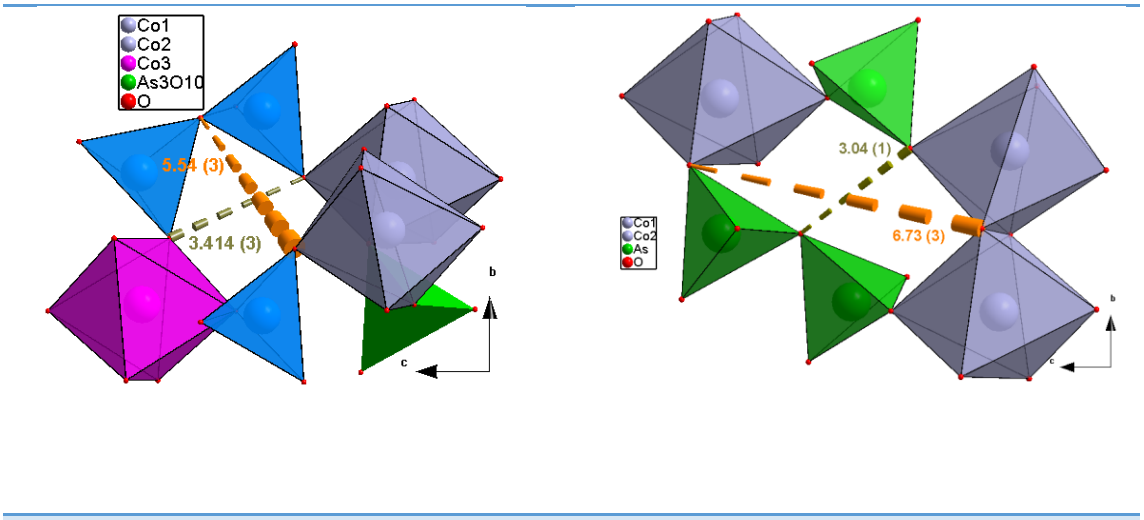

(a)

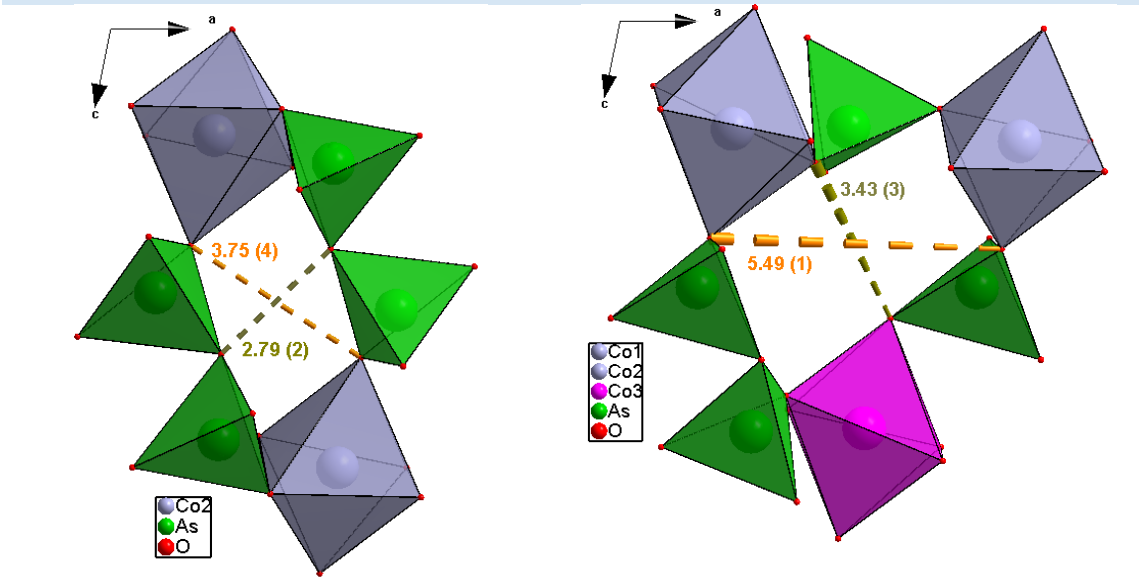

(b)

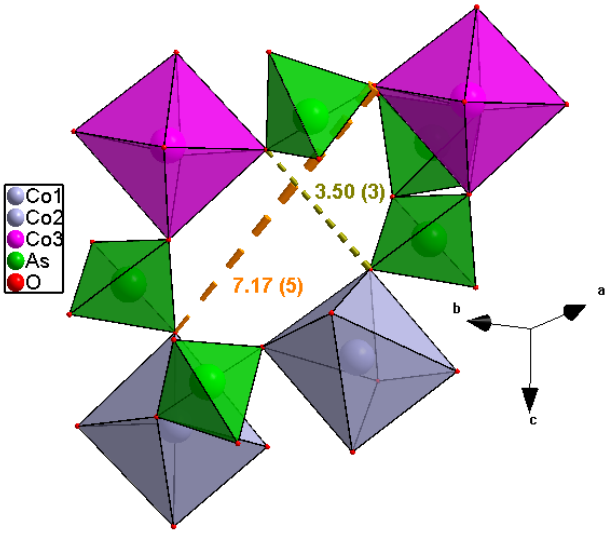

(c)

Figure 8. Dimensions sections of tunnels along (a) [100] (b) [010] (c) [110] axes of $Na_7Li_{0.8}K_{0.2}Co_5(As_3O_{10})_2(As_2O_7)_2$.

The obtained results are close to those encountered for the intermediate conductor $Na_3Bi_2(AsO_4)_3$ (0.85 eV) [34] which the alkali-ions are located in two different tunnels with divers sections on the anionic framework. Indeed, among the sodium cations of the cited materials, the sodium ion, noted Na(1), are the most mobile ion. In fact, the fast mobility is due to the localization of the Na^+ ions in tunnels with relatively wide sections (5.13Å- 5.58Å) compared to those of the second tunnel which is of the order of 3.83 Å - 5.13 Å.

On the other hand, the geometric factors of the tunnels on the anionic framework reveals that the appropriate geometry is not sufficient for fast ionic conduction. In fact, returning to the qualitative calculation of the sodium and oxygen Shannon ionic radii $2[r_{Na+} + r_{O2-}] = 5.18$Å [43], it indicates that the geometric factors of the tunnels in the studied material and in $Na_3Bi_2(AsO_4)_3$ [34] remain relatively insufficient during the way of these tunnels. Therefore, the ionic dispalcement can be partially obstructed and the conduction is expected to be lower.

4. CONCLUSION

Alkali cobalt di-triarsenate, the first in the *A*-Co-As-O systems (*A*= monovalent cation), was synthesized using solid-state reaction method. Based on single crystal diffraction data, the structure can be described as with 3D open framework with tunnels running along [100], [010] and [110] directions where alkali ions are located. The investigation of the monovalent cations conductivity computationally via Bon Valence Site Energy simulation indicate that only sodium ions are mobile in the anionic framework, especially the Na2 ions. In qualitative agreement with the structural characteristics, the BVSE approach pointed to a one dimensional type of Na^+ ions migration along [110] with an activation energy 0.83 (eV) which suggests that fast ionic conductivity may be expected experimentally in subsequent works.

ACKNOWLEDGEMENTS
The authors extend their appreciation to the Deanship of Scientific Research at King Khalid University for funding this work through research groups program under grant number R.G.P.2/46/40.

SUPPORTING DATA
The Crystallographic Information Data File (CIF) containing more details of the crystal structure was deposited in the Cambridge Crystallographic Data Centre (CCDC), 12 Union Road, Cambridge CB2 1EZ, UK; Fax: +44(0)1223-762911; email: deposit@ccdc.cam.ac.uk] (or at www.ccdc.cam.ac.uk/conts/retrieving.html) on quoting the deposit number CCDC 1964181.

References

1. C.A.J. Fisher, V.M. Hart Rrieto and M. Saiful Islam, *Chem. Mater.,* 20 (2008) 5907.
2. G. Li, H. Azuma and M. Tohda, *Electrochem. Solid-State Lett.,* A 5 (2002) 135.

3. A. Yamada, S.C. Chung and K. Hinkuma, *J. Electrochem. Soc.,* A 148 (2001) 224.
4. J.B. Goodenough, H.Y-P. Hong and J.A. Kafalas, *Mater. Res. Bull.,* 11 (1976) 203.
5. S.Y.P. Hong, *Mater. Res. Bull.,* 11 (1976) 173.
6. S.R.S. Prabaharan, M.S. Michael, S. Radhakrishna, and C. Julien, *J. Mater. Chem.,* 7 (1997) 1791.
7. H.Y-P. Hong, *Mater. Res. Bull.,* 11 (1976) 173.
8. A.K. Padhi, K.S. Nanjundaswamy and J.B. Goodenough, *J. Electrochem. Soc.,* 144(4) (1997) 1188.
9. 9. A. Jain, G. Hautier, S.P. Ong, S. Daceka and G. Ceder, *Phys. Chem. Chem. Phys.,* 17 (2015) 5942.
10. H. Boughzala, A. Driss and T. Jouini. *Acta Cryst. C*53 (1997) 3.
11. Y. Ben Smida, R. Marzouki, S. Georges, R. Kutteh, M. Avdeev, A. Guesmi and M.F. Zid, *J. Solid State Chem.* 239 (2016) 8.
12. R. Marzouki, A. Guesmi, S. Georges, M.F. Zid and A. Driss, *J. Alloy. Compd.* 586 (2014) 74.
13. M.V.V.M. Satya Kishore and U.V. Varadaraju, *Mater. Res. Bull.,* 41 (2006) 601.
14. M. Alvarez-Vega, J.M. Gallardo-Amores, F. Garcia-Alvarado and U. Amador, *Solid State Sc.,* 8 (2006) 952.
15. A.J.M. Duisenberg, *J. Appl. Crystallogr.,* 25 (1992) 92.
16. J. Macíček and A. Yordanov, *J. Appl. Crystallogr.,* 25 (1992) 73.
17. A.C.T. North, D.C. Phillips and F.S. Mathews, *Acta Crystallogr., A*24 (1968) 351.
18. G.M. Sheldrick, *Acta Cryst., C*71 (2015) 3.
19. L.J. Farrugia, *J. Appl. Crystallogr.,* 32 (1999) 837.
20. K. Brandenburg and M. Berndt, *Diamond Version 2.1* (2001) Crystal Impact. Bonn.
21. S. Adams, *softBV* (2003) University of Gottingen, Germany. http://www.softbv.net
22. M. Nespolo and B. Guillot, *J. Appl. Cryst.,* 49 (2016) 317.
23. S. Adams and R.P. Rao, *Bond Valences,* (2014) 129.
24. L. Pauling, *J. Am. Chem. Soc.,* 51 (1929) 1010.
25. I.D. Brown and D. Altermatt, *Acta Cryst., B*41 (1985) 244.
26. D. Mazza, *J. Solid State Chem.*, 156 (2001) 154.
27. R. Marzouki, Y. Ben Smida, M. Avdeev, Majed M. Alghamdi, M.F. Zid, *Mater. Res. Express,* 6 (2019) 126313.
28. M.A. Ben Moussa, R. Marzouki, A. Brahmia, S. Georges, S. Obbade and M.F. Zid, *Int. J. Electrochem. Sci.,* 14 (2019) 1500.
29. W.H. BAUR, *Acta Cryst*., B30 (1974) 1195-1215.
30. M. Wildner, *Zeitschrift für Kristallographie - Crystalline Materials*, 202 (1992), 51.
31. B. Ayed, A. H. Abbdallah, A. Hadded, *Acta Cryst., E 60* (2004) i52.
32. W. Frigui, C. Falah, H. Boughzala, M. F. Zid, A. Driss, *J. Soc. Chim. Tunisie,* 12 (2010) 179.
33. S. Bdeya , N. F. Bourguiba , S. N. Savvin , P. Núñez, *J. Solid State Chem.,* 272 (2019) 189.
34. S. Bdeya , N. F. Bourguiba , S. N. Savvin , C. Falah, M.F. Zid, P. Núñez, *J. Alloy. Compd.* 762 (2018) 806.
35. S. Bdeya , N. F. Bourguiba , S. N. Savvin , M.F. Zid, P. Núñez, *J. Solid State Chem.,* 276 (2019) 382.
36. R. Nasri, R. Marzouki, S. Georges, S. Obbade and M.F. Zid, *Turk. J. Chem.,* 42 (2018) 1251.
37. R. Marzouki, Y. Ben Smida, A. Guesmi, S. Georges, I.H. Ali, S. Adams and M.F. Zid, *Int. J. Electrochem. Sci.,* 13 (2018) 11648.
38. R. Marzouki, A. Guesmi, M.F. Zid and A. Driss, *Crystal Structure Theory and Applications,* 1 (2013) 68.
39. R. Marzouki, A. Brahmia, S. Bondock, M.F. Zid, Sherif M.A.S. Keshk, A. Koschella, T. Heinze, *Carbohydr. Poly.,* 221 (2019) 29.
40. R. Marzouki, Y. Ben Smida, M. Sonni, M. Avdeev, M.F. Zid, *J. Solid State Chem.,* in press, https://doi.org/10.1016/j.jssc.2019.121058
41. R. Marzouki, A. Guesmi, M.F. Zid, A. Driss, *Ann. Chim. Sci. Mat.,* 38 (3-4) (2013) 117.

42. Y. Ben Smida, R. Marzouki, A. Guesmi, S. Georges, M.F. Zid, *J. Solid State Chem.,* 221 (2015) 132.
43. R. D. Shannon. *Acta Crystallogr*., 32 (1976) 751.